Journal of Solid State Electrochemistry (2020) 24:545–555
https://doi.org/10.1007/s10008-019-04468-2

ORIGINAL PAPER

Preparation and characterization of Ti/SnO_2-Sb_2O_3/α-PbO_2/Ce-Nd-β-PbO_2 composite electrode for methyl orange degradation

Yufu Pan[1] · Yanfang Luo[1] · Chengcheng Li[1] · Rongjing Wang[1] · Yihao Yuan[1] · Meng Li[1] · Ping Na[1]

Received: 5 October 2019 / Revised: 2 December 2019 / Accepted: 7 December 2019 / Published online: 9 January 2020

Abstract

The present study focused on the preparation, characterization, and application of cerium (Ce) and neodymium (Nd) co-doped lead (PbO_2) electrode, i.e., Ti/SnO_2-Sb_2O_3/α-PbO_2/Ce-Nd-β-PbO_2. The electrochemical activities of the modified electrode were investigated and compared with those of Ce-PbO_2, Nd-PbO_2, and pure PbO_2 electrodes. Scanning electron microscopy (SEM), energy-dispersive X-ray spectroscopy (EDX), X-ray diffraction (XRD), and X-ray photoelectron spectroscopy (XPS) were used to characterize the surface morphology, crystal structure, and elemental states of the modified electrode. The Ce and Nd co-doped PbO_2 electrode had smaller crystal particles, more compact structure, and higher activity of electrocatalysis compared with the single-doped and undoped PbO_2 electrodes. Linear sweep voltammetry (LSV) and electrochemical impedance spectroscopy (EIS) were also utilized to study the electrochemical response of the modified electrodes. The results show that the prepared Ce-Nd-PbO_2 electrode has the highest O_2 evolution potential (OEP) and lowest charge transfer resistance, suggesting that it has the lower energy consumption than the other three kinds of electrodes. Electrochemical oxidation methyl orange (MO) as a model dye wastewater was studied to evaluate the potential applications of this modified electrode in environmental science. It was found that the Ce-Nd-PbO_2 electrode exhibited higher MO and chemical oxygen demand (COD) removal efficiency than single-doped and pure PbO_2 electrodes.

Keywords Electrochemical advanced oxidation processes · PbO_2 electrode · Cerium · Neodymium · Methyl orange

Introduction

With the rapid development of textile and printing leather industry, a large amount of printing and dyeing wastewater is discharged into the water environment every year [1, 2]. Most dyes are persistent organic pollutants, characterized by high concentration and high toxicity [3, 4]. So, effective control and treatment of the dye wastewater has become an urgent problem to be solved. Methyl orange is a complex azo organic compound, widely used in printing and dyeing, and textile and material coloring as a coloring agent. Methyl orange has good stability and is not easily degraded under natural conditions, so it is necessary to expand its degradation methods [5]. Traditional treatment methods for dye wastewater mainly include coagulation, biological oxidation, adsorption, ion exchange, and chemical oxidation [6–8]. However, meeting the more and more strict discharge standard of dye wastewater treatment is difficult for these methods.

Recently, electrochemical advanced oxidation processes (EAOPs) have gained increasing attention as a promising method for wastewater treatment [9–16]. It has the advantages of strong oxidation ability, good environmental compatibility, high energy efficiency, and cost effectiveness. Anodic oxidation (AO) is the simplest EAOP; it includes direct anodic oxidation by electron transfer to the anode (M) surface and indirect oxidation by the powerful physisorbed M(·OH) at the electrode surface produced by Eq. (1) [17]. And the organics are oxidized to CO_2 by the highly reactive M(·OH) (2). The efficiency of AO is highly dependent on the mass transfer of pollutants from the bulk to the electrode surface or its vicinity [18]. Besides, the electrode material nature also has strong influence on both efficiency and selectivity of AO. There are

✉ Ping Na
naping@tju.edu.cn

[1] School of Chemical Engineering and Technology, Tianjin University, Tianjin 300354, China

two types of electrode materials used for AO, the active electrodes and the non-active electrodes; the former one has low oxygen evolution potential (OEP), in which the M(·OH) is transformed into a higher state oxide or superoxide that in combination with the anode surface M acts as a selective mediator in the oxidation of organics, and the latter one has high OEP, in which M(·OH) are so weakly physisorbed at the electrode surface that can react with organics. As a general rule, the higher the potential for oxygen evolution of the electrode material, the weaker the interaction of M(·OH) with the electrode surface and the higher the chemical reactivity toward organics oxidation [17].

$$M + H_2O \rightleftarrows M(\cdot OH) + H^+ + e^- \quad (1)$$

$$\text{Organics} + M(\cdot OH) \rightleftarrows CO_2 + H_2O \quad (2)$$

The typical active electrodes include platinum (Pt), graphite, ruthenium dioxide (RuO_2), and iridium dioxide (IrO_2); generally speaking, their potentials for O_2 evolution are lower than 1.8 V/SHE. On the other hand, lead dioxide (PbO_2), tin dioxide (SnO_2), and boron-doped diamond (BDD) can be considered non-active electrodes, whose potentials of O_2 evolution are from 1.7 to 2.6 V/SHE. The BDD electrode is the most effective non-active electrode at present [19, 20], which is considered to be the most suitable electrode for AO. However, its application is severely restricted by its high cost. As a promising electrode material, PbO_2 has gained more and more attention because of its high electrical conductivity, strong oxidation ability, large surface area, and low cost [21].

Compared with those by other chemical methods, the PbO_2 layers prepared by electrodeposition have higher electrochemical activity. Meanwhile, the morphology and crystalline structures of electrodeposited PbO_2 are related to many factors, such as the type of substrate, electrodeposition process, pH of the electrodeposition solution, and type of dopants. The common substrates used for the deposition of PbO_2 films mainly include Ti, Pb, Pt, Ta, C, and TiO_2 [22–31]. Titanium was used as the substrate in this study due to its natural corrosion resistance; in addition, Ti is also preferred because it strongly passivates under high positive potentials in the case of any local failure of the PbO_2 layer during electrolysis.

Recently, a lot of researches afford to increase the chemical stability and electrocatalytic capacity of PbO_2 by doping modification. Some metal ions like nickel, iron, neodymium, bismuth, cobalt, and cerium have been used for modification of PbO_2 electrode as dopants by the electrodeposition method [4, 32–34]; besides, some metal oxides were also doped into PbO_2 electrodes such as CeO_2, ZrO_2, Sm_2O_3, TiO_2, and Ga_2O_3 [35–48]. Cerium is a promising candidate to modulate the electrocatalytic properties of oxide electrodes due to its high Ce(III)/Ce(IV) redox potential.

The aim of this work focuses on the investigation of electrochemical activity and stability of lead dioxide electrode co-doped with cerium and neodymium, i.e., Ti/Ce-Nd-PbO_2. The electrochemical activities of the modified electrode were investigated and compared with Ce-PbO_2, Nd-PbO_2, and undoped PbO_2 electrodes. Different doping ratios of cerium and neodymium were studied and the optimum ratio was determined. Analysis techniques such as SEM, XRD, and XPS were used to characterize the modified electrode. Linear sweep voltammetry (LSV), electrochemical impedance spectroscopy (EIS), and accelerated life test were also used to study the electrochemical properties of Ti/Ce-Nd-PbO_2. Moreover, UV-visible and COD were used to investigate dye removal and mineralization. The anodic oxidation of methyl orange as a model dye wastewater was examined to determine the optimum operating parameters of the Ti/Ce-Nd-PbO_2 electrodes for degradation of organic pollutants.

Experiment and methodology

Materials

All the reagents and materials used in this work were of analytical grade without further purification. Cerium and neodymium tri-nitrate, lead and copper di-nitrate, sodium sulfate, oxalic acid, nitric acid, sodium hydroxide, lead oxide, sulfuric acid, methyl orange, and sodium fluoride were obtained from Aladdin Reagent Company. Distilled water (DI water) was used throughout the work.

Electrode preparation and characterization

The main preparation procedure is shown in Fig. 1. High-purity (99.7%) titanium sheets (2.0 cm × 3.0 cm × 0.08 cm) were used as the substrate. Firstly, titanium sheets were mechanically polished by abrasive paper, then were rinsed in ethanol and DI water by ultrasonic washing, and after that, were cleaned by degreasing in 40 wt% NaOH solution at 358.15 K for 30 min and etching in boiled 10 wt% oxalic acid for 1 h to attain the uniform roughness on the surface of electrodes. Finally, the titanium sheets were rinsed carefully using DI water with ultrasonic [49].

After pretreatment, an interlayer of Ti/SnO_2-Sb_2O_3 and α-PbO_2 between the Ti substrate and surface active layer was prepared to improve the stability and extend the life of PbO_2 electrodes. In this step, dip-coating and thermal deposition of $SnCl_4 \cdot 5H_2O$, $SbCl_3$, *n*-butanol, and hydrochloric acid with a molar ratio of Sn:Sb = 8:1 were used. The pretreated titanium sheets were painted, dried, and sintered at 773 K in a muffle furnace. This same procedure was repeated ten times. The SnO_2-Sb_2O_3 interlayer was finally obtained by last baking at 773 K for 1 h. Then, an interlayer of α-PbO_2 was electrodeposited using the Ti/SnO_2-Sb_2O_3 as an electrode and a Pt plate as a cathode in alkaline solution (0.1 mol L^{-1} PbO,

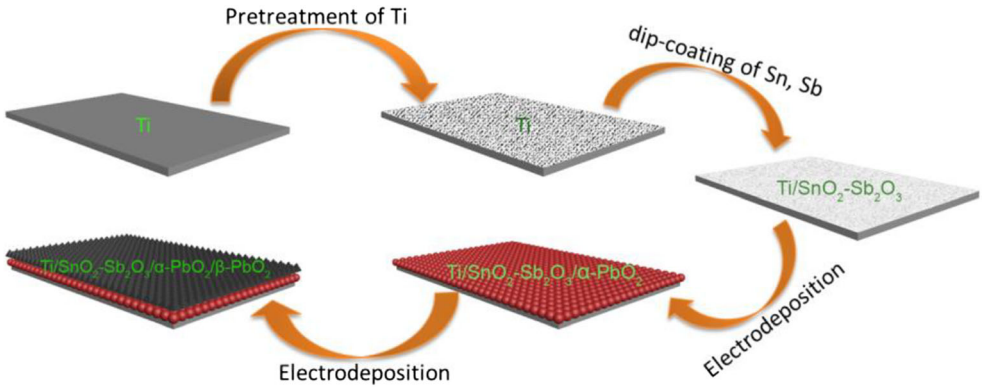

Fig. 1 Preparation procedure of Ti/SnO_2-Sb_2O_3/α-PbO_2/β-PbO_2 electrode

3.5 mol L^{-1} NaOH) at 313.15 K and a current density of 10 mA cm^{-2} for 2 h. Finally, the surface active layer β-PbO_2 was further electrodeposited on the above-prepared Ti/SnO_2-Sb_2O_3/α-PbO_2 substrate in acidic solution that consisted of 0.2 mol L^{-1} $Cu(NO_3)_2$, 40 mmol L^{-1} NaF, 0.5 mol L^{-1} $Pb(NO_3)_2$, and 0.1 mol L^{-1} HNO_3 for pure PbO_2 electrode, whereas 0.3 g L^{-1} of $Ce(NO_3)_3$ and $Nd(NO_3)_3$, respectively, was used for Ce- and Nd-doped PbO_2 electrodes. Furthermore, the nominal compositions of Ce:Nd = 1:1, 1:2, 2:1, 1:5, 5:1, respectively, were used for the electrodeposition of Ce-Nd co-doped PbO_2 electrodes, and the total concentration of Ce and Nd was 0.3 g L^{-1}. In addition, pure PbO_2 and single-doped and co-doped PbO_2 electrodes were all deposited within 2 h at 333.15 K and 20 mA cm^{-2} current density.

A scanning electron microscope (SEM; Hitachi-SU8010, Japan) was used to characterize the morphology of the surface. This instrument incorporated an energy-dispersive X-ray analysis (EDX) for elemental analysis. X-ray diffraction (XRD) was used to examine the crystalline structures of the modified PbO_2 electrodes, which were recorded on an X-ray diffraction instrument (D8Focus, Bruker AXS, Germany) under Cu Kα radiation (45 kV, 30 mA) with a scanning range from 20° to 80° at the speed of 8°/min. X-Ray photoelectron spectroscopy (XPS, PHI5000VersaProbe, Ulvac-Phi) was used to determine the atomic valence state by using the Mg Ka X-ray source with a base vacuum operated at 300 W.

The electrochemical characterization of the modified PbO_2 electrodes was performed by linear sweep voltammetry (LSV) and electrochemical impedance spectroscopy (EIS) measurements using an electrochemical workstation (CHI660E, China) with standard three-electrode configuration. PbO_2, platinum, and saturated calomel electrodes (SCE) were used as the working electrode, the counter electrode, and the reference electrode, respectively. The LSV measurements were made in 0.5 mol L^{-1} Na_2SO_4 solution. The curves were recorded from 0 to 2.0 V with a scanning rate of 5 mV/s, and the potential corresponding to the inflection point of polarization curve was defined as the oxygen evolution potential (OEP) of the electrodes. The EIS measurements were made in 0.5 mol L^{-1} Na_2SO_4 solution, and the open-circuit potential was used as the measurement potential. The frequencies swept were from 100 KHz to 100 mHz with an applied sine wave of 10-mV amplitude. The accelerated life of the modified PbO_2 electrodes was tested in 1.0 mol L^{-1} H_2SO_4 at $j = 2.0$ A cm^{-2} and 333 K to assess the stability of electrodes.

Experiment method and analysis

An open glass reactor of 100-mL capacity connected with a DC power supply (IT6332L, ITECH, China) was used for the electrochemical oxidation experiments of methyl orange. The different modified PbO_2 electrodes were used as anodes while the Ti plate was used as the cathode, and the interelectrode gap was kept at 1.0 cm in our experiments. A 100 mL solution of 60 mg L^{-1} methyl orange was placed in the reactor under continuous stirring of 400 rpm on a magnetic stirrer [50]. Samples were analyzed after being drawn at certain intervals. The AO process was optimized with the Ce-Nd-PbO_2 electrode at different parameters such as current density (j) (5–30 mA cm^{-2}), initial methyl orange concentration (C_0) (30–120 mg L^{-1}), and initial solution pH (2–11), respectively, at room temperature. The 0.5 mol L^{-1} H_2SO_4 and NaOH solutions were used to adjust the pH of the solution in the experiment.

UV-Vis absorption spectra of methyl orange solution were recorded on UV-Vis spectrophotometer (Lambda 35, PerkinElmer) at 465 nm. And the COD was measured by the COD detector (6B-200, SHENGAOHUA, China). The MO and COD removal can be calculated via Eqs. (3) and (4), respectively.

$$\text{MO removal} = \frac{A_0 - A_t}{A_0} \times 100\% \tag{3}$$

A_0 and A_t are the initial and final absorbances of MO.

$$\text{COD removal} = \frac{COD_0 - COD_t}{COD_0} \times 100\% \tag{4}$$

COD_0 and COD_t are the initial and final concentrations of

COD ($mgO_2\ L^{-1}$).

The average current efficiency (ACE, ζ) was calculated by Eq. (5) from the COD results [51].

$$\varsigma = \frac{(\mathrm{COD}_0 - \mathrm{COD}_t)\cdot F \cdot VL}{8I\cdot \Delta t \cdot 1000} \times 100(\%) \quad (5)$$

where COD_0 and COD_t are the initial and final concentrations of COD ($mgO_2\ L^{-1}$), F is the Faraday constant (96,487 C mol^{-1}), V_L is the volume of electrolyte solution (L), Δt is the degradation time (s), and I is the current intensity (A).

A well-fitted pseudo-first-order kinetic of MO dye degradation was determined by using the following expression:

$$\ln\left(\frac{C_0}{C_t}\right) = kt \quad (6)$$

where C_0 and C_t are the initial and final absorbances of MO, and k is the reaction rate constant.

Results and discussion

Effect of $Ce(NO_3)_3$ and $Nd(NO_3)_3$ concentrations in deposition bath on electrocatalytic activity of PbO_2 electrodes

Initial experiments were carried out to optimize the proportion of Ce and Nd in the electrodeposition bath of Ce-Nd co-doped PbO_2 electrodes in terms of MO and COD removal. The total concentration of $Ce(NO_3)_3$ and $Nd(NO_3)_3$ was 0.3 g L^{-1}, and Ce:Nd = 1:1, 1:2, 2:1, 1:5, and 5:1 were defined as Ce-Nd-PbO_2-1, Ce-Nd-PbO_2-2, Ce-Nd-PbO_2-3, Ce-Nd-PbO_2-4, and Ce-Nd-PbO_2-5, respectively. The electrolysis processes were performed at the condition of 60 mg L^{-1} MO, room temperature, 20 mA cm^{-2} current density, 0.15 mol L^{-1} Na_2SO_4 concentration, and pH = 7. Figure 2 shows the effect of different concentrations of $Ce(NO_3)_3$ and $Nd(NO_3)_3$ in electrodeposition bath on MO removal, as well as the kinetics of degradation. As can be seen in the graph, a linear relationship between removal efficiency as a function of treatment time depicted by MO on different electrodes followed the pseudo-first-order kinetic. Compared with the PbO_2 electrode, single-doped and different proportions of Ce-Nd co-doped PbO_2 electrodes have been observed to show the higher MO removals in this chart. Furthermore, the Ce-Nd-PbO_2-2 electrode, which has a content of 0.1 g L^{-1} $Ce(NO_3)_3$ and 0.2 g L^{-1} $Nd(NO_3)_3$ in the electrodeposition bath, shows the highest MO removal in the shortest time. About 99.8% was formed with Ce-Nd-PbO_2-2 electrode after 70 min of electrolysis compared with 98.7%, 99.1%, and 97.1% with Ce, Nd-PbO_2, and PbO_2 electrodes, respectively. The COD removal and the average current efficiency are shown in Fig. 3; similar to the result of the MO removals, higher COD removals were shown with all of the doped PbO_2 electrodes over the undoped PbO_2 electrode, and the Ce-Nd-PbO_2-2 electrode also shows the highest COD removal, as well as the highest average current efficiency. Almost 100% COD

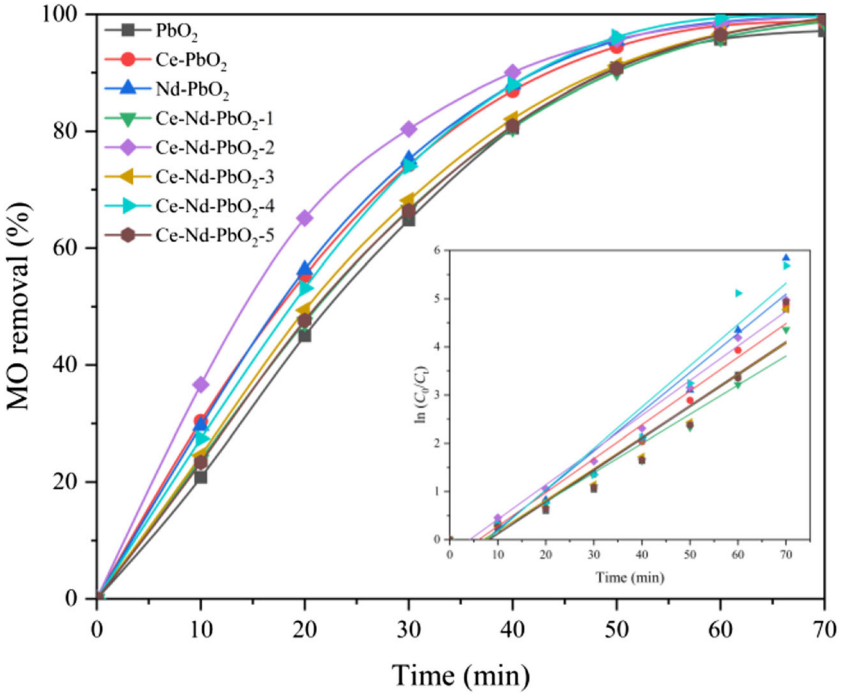

Fig. 2 Effect of different concentrations of $Ce(NO_3)_3$ and $Nd(NO_3)_3$ in electrodeposition bath on MO removal and the kinetics of degradation at 60 mg L^{-1} MO, room temperature, 20 mA cm^{-2} current density, 0.15 mol L^{-1} Na_2SO_4 concentration, pH = 7, and 70-min treatment time

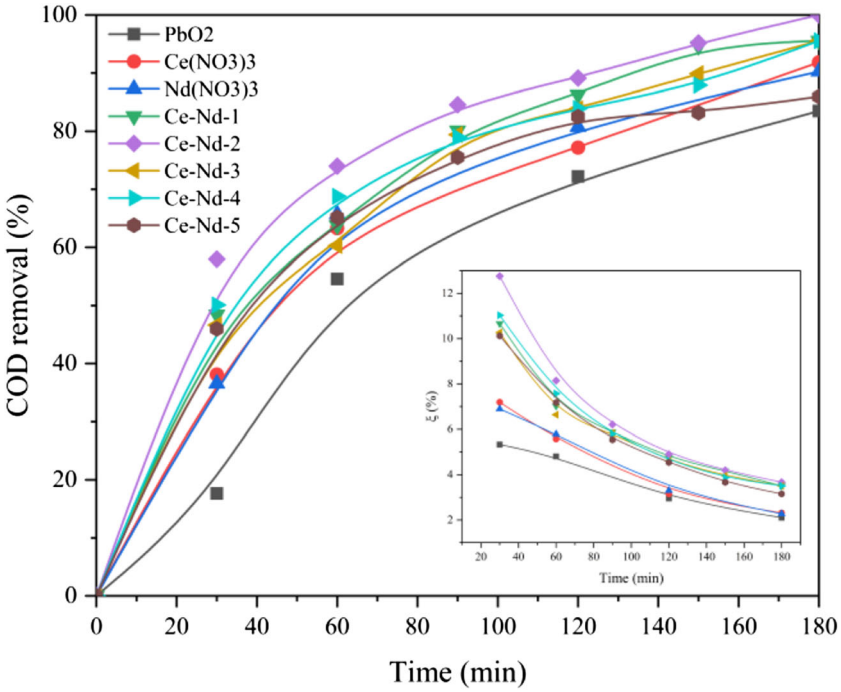

Fig. 3 Effect of different concentrations of $Ce(NO_3)_3$ and $Nd(NO_3)_3$ in electrodeposition bath on COD removal and the ζ versus treatment time at 60 mg L^{-1} MO, room temperature, 20 mA cm^{-2} current density, 0.15 mol L^{-1} Na_2SO_4 concentration, pH = 7, and 180-min treatment time

removal was reached with Ce-Nd-PbO_2-2 electrode after 180 min of electrolysis, which was higher compared when using the other electrodes, such as 91.8% with the Ce-PbO_2 electrode, 90.2% with the Nd-PbO_2 electrode, and 83.4% with the undoped PbO_2 electrode. For MO removal, COD removal, and the average current efficiency, it was reasonable to conclude that Ce and Nd co-doping under suitable conditions helps to improve the electrode performance, and the Ce-Nd-PbO_2–2 electrode that contains 0.1 g L^{-1} $Ce(NO_3)_3$ and 0.2 g L^{-1} $Nd(NO_3)_3$ can be chosen as the best Ce-Nd co-doped PbO_2 electrode for methyl orange degradation. The Ce-Nd-PbO_2–2 electrode

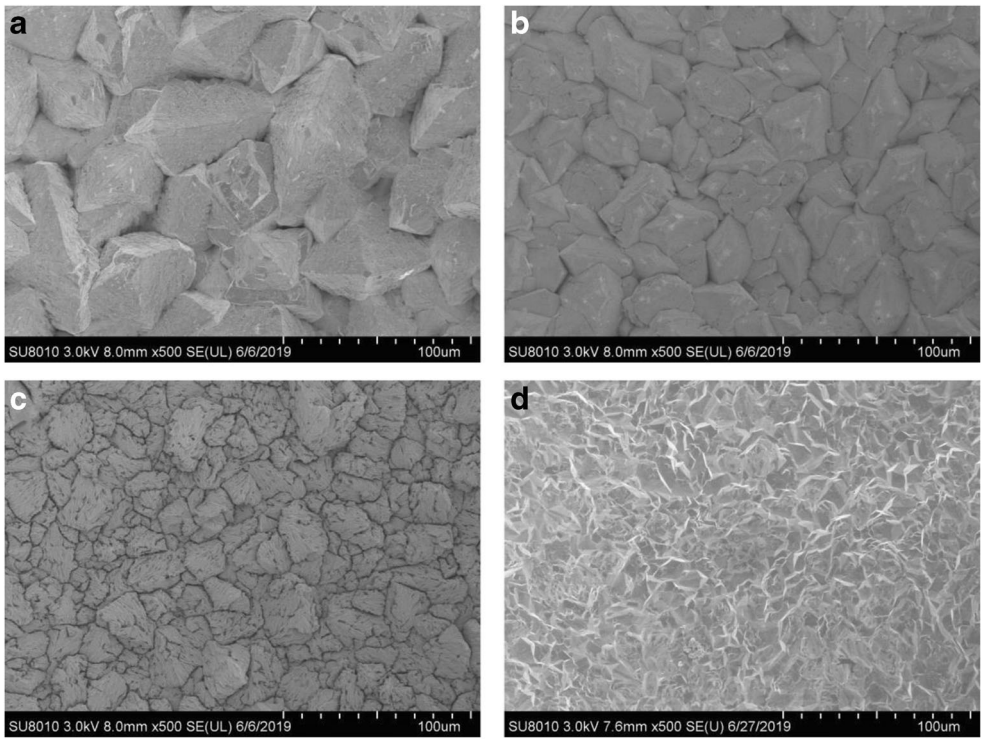

Fig. 4 SEM images of different PbO_2 electrodes: **a** Ti/PbO_2, **b** Ti/Ce-PbO_2, **c** Ti/Nd-PbO_2, and **d** Ti/Ce-Nd-PbO_2 electrodes

was redefined to Ce-Nd-PbO_2 electrode used in the later experiments.

Morphologies and crystal structure of PbO_2 electrodes

The SEM micrographs of Ti/PbO_2, Ti/Ce-PbO_2, Ti/Nd-PbO_2, and Ti/Ce-Nd-PbO_2 electrodes are shown in Fig. 4. PbO_2 surface had a pyramidal cluster-like morphology with many cracks. This structure may be caused by the dropping of PbO_2 from Ti substrate which may shorten the service life of PbO_2 electrodes [45]. The Nd and Ce-PbO_2 were found to be quite similar, and their crystal particles were smaller than that of PbO_2 electrode. However, the morphology of PbO_2 and Ce-Nd-PbO_2 electrode was also found to be slightly similar, but the crystal of Ti/Ce-PbO_2 electrode was smaller and the structure was more compact than that of no-doped and single-doped PbO_2 electrodes. The doping of Ce and Nd into PbO_2 significantly affected the film morphology, and the Ce-Nd-PbO_2 electrode has a higher catalytic activity because of its larger effective area than the other PbO_2 electrodes. Furthermore, the surface of PbO_2 electrode that was doped with Ce and Nd became denser and smoother, and that would be favorable to prevent reactive oxygen species from diffusing into the internal layer in the process of electro-oxidation, improving the stability and the service life of electrodes [37].

Figure 5 shows the EDX results of Ti/PbO_2 (Fig. 5a) and Ti/Ce-Nd-PbO_2 (Fig. 5b) electrodes. It can be found that the real atomic percentage of Ce in the surface of Ti/Ce-Nd-PbO_2 electrode was 1.77%, and the Nd was 1.899% (data not shown).

Figure 6 shows the XRD patterns of the different modified PbO_2 electrodes, which are in good arrangement with the JCPDS file (card number 75-2417). No diffraction peak corresponding to CeO_2 or Nd_2O_3 was observed; this may be due to the low content of Ce and Nd. By the way, the main diffraction peaks of the electrodes were β-PbO_2. The peaks of doped PbO_2 electrodes are identical to that of pure PbO_2 without any shift, meaning that the addition of Ce and Nd would not change the phase of the PbO_2 electrode. However, compared to the pure PbO_2 electrode, the intensities of some peaks of doped electrodes were significantly changed, such as the typical peak at 36.9° which can be found stronger with the dope of Nd and most peaks of Ce-Nd-PbO_2 electrode were significantly smaller, suggesting the existence of Ce and Nd onto modified PbO_2 electrode and this may have an effect on the growth and structure of the crystal.

In order to further delve into the chemical composition of the different PbO_2 electrodes, XPS of the doped PbO_2 electrodes was conducted as shown in Fig. 7. The Pb 4f

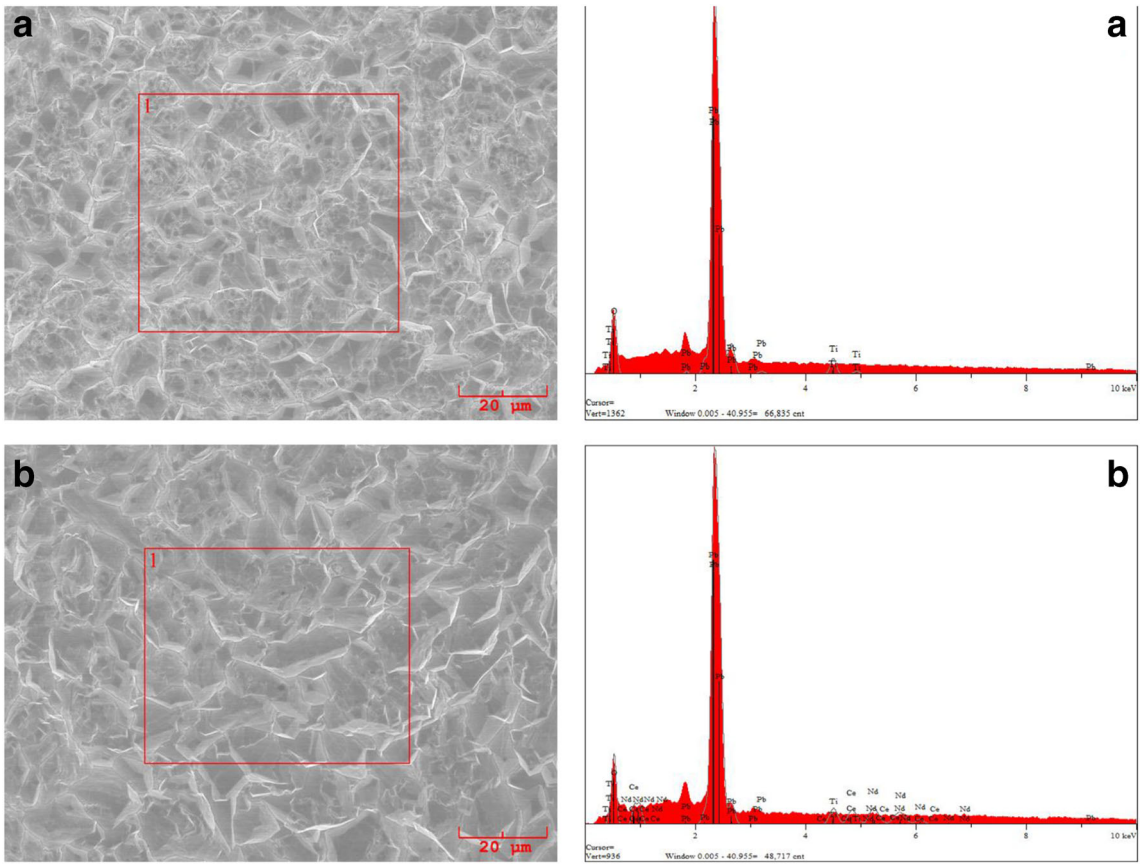

Fig. 5 EDX images of **a** PbO_2 electrode and **b** Ce-Nd-PbO_2 electrode

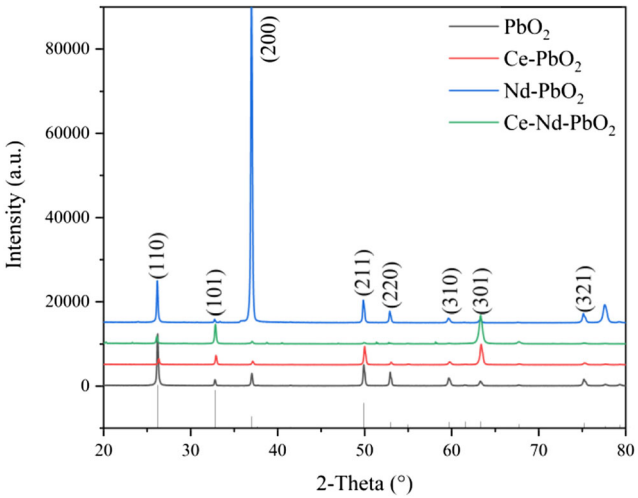

Fig. 6 X-Ray diffraction patterns of different modified PbO_2 electrodes

spectrum (Fig. 7a) presents two well-defined and symmetric peaks centered at 137.5 eV and 142.6 eV, which can be attributed to Pb $4f_{5/2}$ and Pb $4f_{7/2}$, respectively, in agreement with the spectral values for PbO_2. The O1s spectrum (Fig. 7b) fitted into a sharp peak at 529.1 eV, which corresponded to strongly bound (lattice) oxygen. Moreover, the binding energies of Ce $3d_{5/2}$ and Ce $3d_{3/2}$ are located at 895.2 and 935.2 eV (Fig. 7c), which indicated that Ce ion of CeO_2 was successfully introduced onto the surface of PbO_2 electrode. The peaks at 978.68 eV and 998.93 eV corresponding to Nd $3d_{5/2}$ and Nd $3d_{3/2}$, which illustrates that the Nd atoms were also successfully introduced at PbO_2 surface, and the Nd $3d_{5/2}$ peak at 978.68 ev suggested a good correlation with Nd^{3+} oxidation state in Nd_2O_3.

Generally speaking, the stability of electrode is an important property in practical application, and it is usually influenced by the dropping of PbO_2 from Ti substrate due to the preparation conditions. In addition, the stability of PbO_2 electrode can be measured by the accelerated life test. Figure 8 shows the accelerated life of the modified PbO_2 electrodes which were tested in 1.0 mol L^{-1} H_2SO_4 at $j = 2.0$ A cm^{-2} and 333 K. The electrolysis time when the potential reached 10 V was regarded as the service life of the electrode. As can be seen in the chart, the service lifetimes of Ce-PbO_2, Nd-PbO_2, Ce-Nd-PbO_2, and the pure PbO_2 electrodes were 87, 82, 95, and 76 h, respectively, which is in good agreement with the previous research.

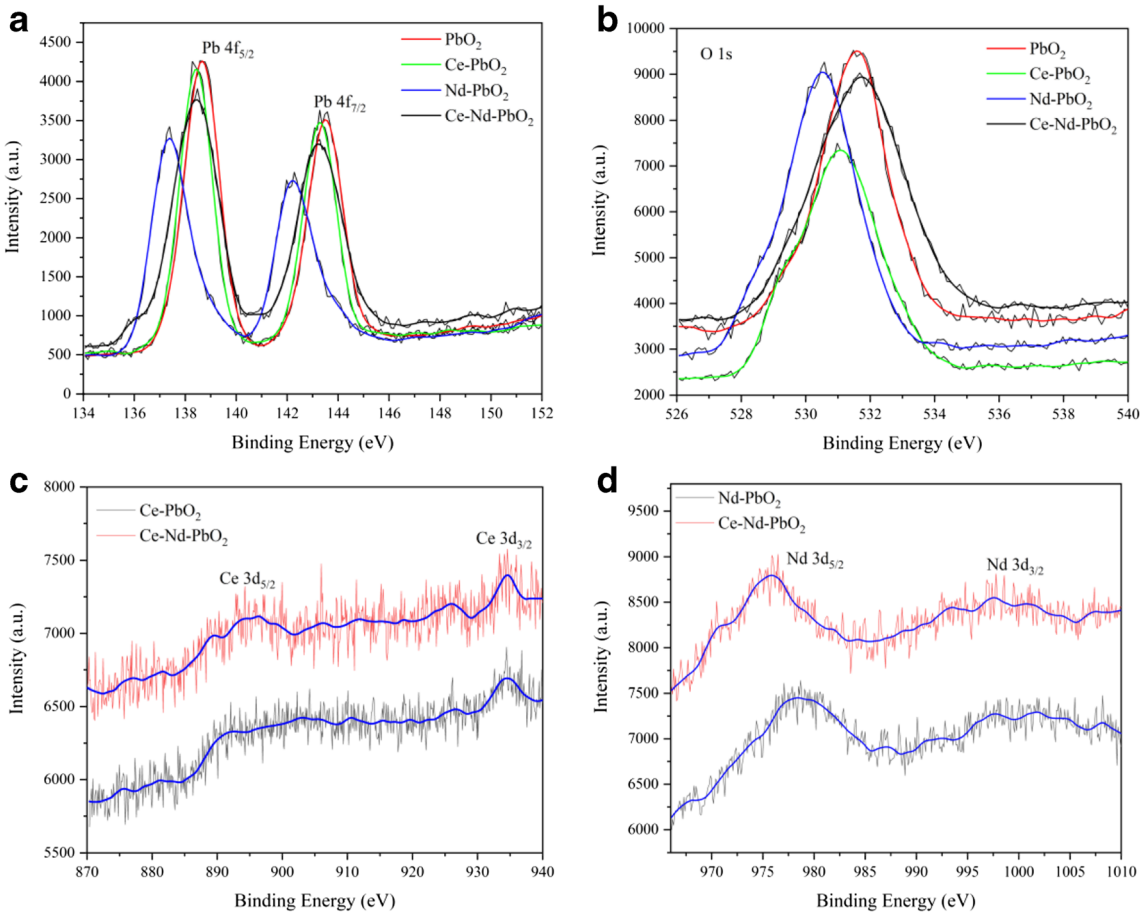

Fig. 7 XPS spectra of different modified PbO_2 electrodes: **a** Pb 4f; **b** O1s; **c** Ce 3d; **d** Nd 3d

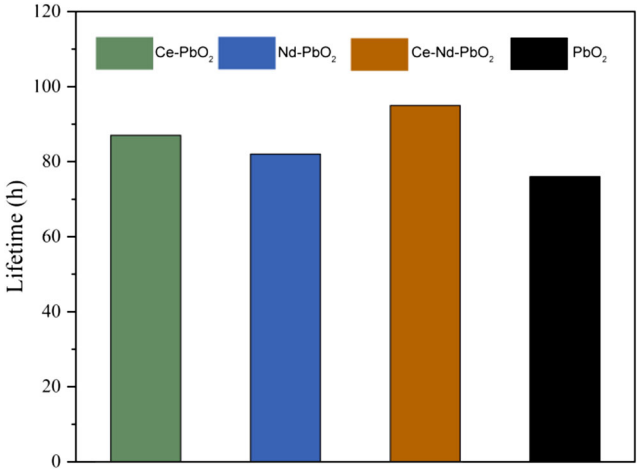

Fig. 8 Accelerated lifetime test in 1.0 mol L^{-1} H_2SO_4 at $j = 2.0$ A cm^{-2} and 333 K

Electrochemical measurements

Figure 9 shows the linear polarization curves obtained in 0.15 mol L^{-1} Na_2SO_4 using Ti/PbO_2, Ti/Ce-PbO_2, Ti/Nd-PbO_2, and Ti/Ce-Nd-PbO_2 electrodes. The intersection of the two almost linear regions at low and high potentials was defined as the onset potential of the electrodes. As observed in the graph, the onset potential of the Ce-Nd-PbO_2 electrode was 2.17 V, which is much higher than that of PbO_2 (1.6 V), Ce-PbO_2 (1.8 V), and Nd-PbO_2 (1.65 V). As a general rule, the higher the onset potential of the electrode material, the weaker the interaction of M(·OH) with the electrode surface and the higher the chemical reactivity toward organics oxidation [17]. On the other hand, high onset potential can effectively reduce energy consumption [52]. Therefore, the Ce-Nd-PbO_2 electrode has the highest chemical reactivity toward organics oxidation.

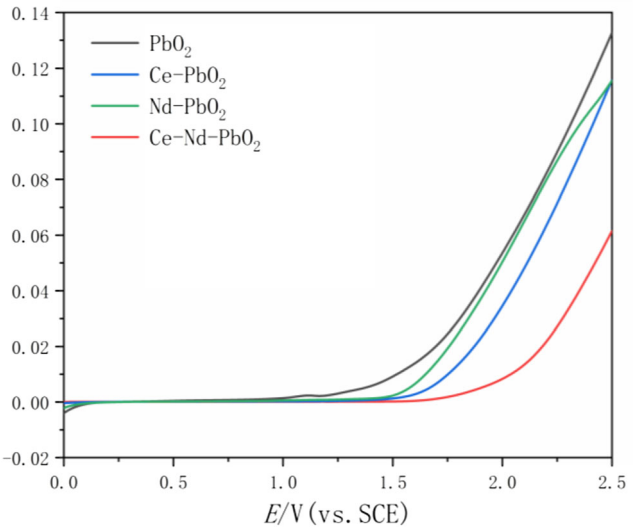

Fig. 9 Linear sweep voltammetry of the different modified PbO_2 electrodes in 0.15 mol L^{-1} Na_2SO_4, scan rate = 100 mV/s

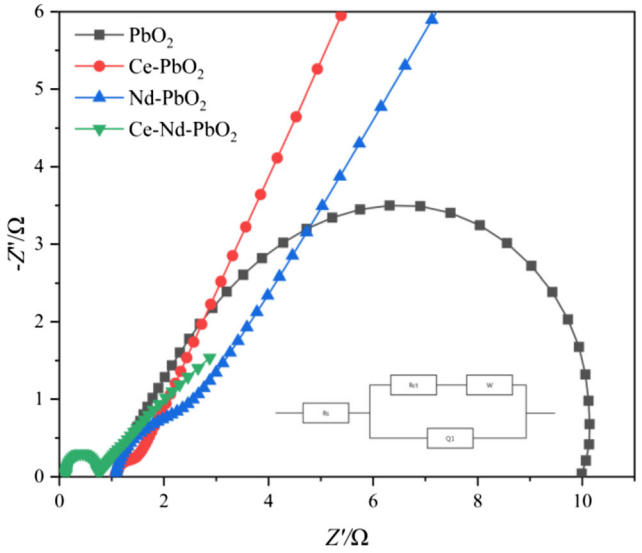

Fig. 10 Electrochemical impedance spectroscopy of different modified PbO_2 electrodes in 0.15 mol L^{-1} Na_2SO_4

The electrochemical impedance spectroscopy measurements were undertaken to study the electrochemical properties of the different doped electrodes. Figure 10 presents the Nyquist plots for these doped electrodes, and EIS simulation results were obtained by fitting experimental data using an equivalent circuit model. In this circuit, Rs presents the solution resistance, Q1 (CPE1) is the constant phase element for double-layer, and Rct is the charge transfer resistance. For the Warburg impedance (*W*), due to mass transfer of ions in surface film, its impedance behavior is displayed in the low frequency.

From the EIS Nyquist plots, we can see that pure PbO_2 electrodes display the biggest arc radius, and Ce-Nd-PbO_2 electrodes display the smallest arc radius among all the electrodes, suggesting the highest charge transfer resistance across pure PbO_2, which signifies that the interfacial charges transfer more rapidly when modified PbO_2 with Ce and Nd.

Optimization of process parameters

Effect of initial pH

Some studies have shown the important role that solution pH plays in the anodic oxidation of dye degradation, but the results are so different due to the different nature of pollutants and electrode materials [53–57]. The effect of initial pH values ranging from 2 to 11 on MO degradation is presented in Fig. 11. H_2SO_4 and NaOH solutions were used for pH adjustments. It can be seen from the figure that the MO removals were increased by increasing the pH from 2.0 to 7.0; then, as the pH increases, it shows a downward trend. So, pH = 5 was chosen as a suitable pH for the further studies.

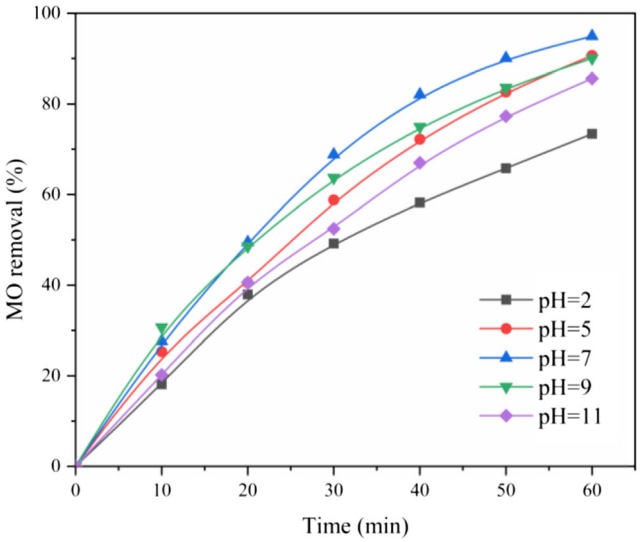

Fig. 11 Effect of initial pH on the MO degradation at 20 mA cm^{-2} current density, 60 mg L^{-1} initial concentration, 0.15 mol L^{-1} Na_2SO_4 concentration, and 60 min of electrolysis time

Effect of applied current density

Figure 12 shows the effect of current density from 5 to 30 mA cm^{-2} on MO removal as a function of treatment time. One can see that the MO removals were dramatically increased as the current density increases from 5 to 20 mA cm^{-2}; however, when the current density increases from 20 to 30 mA cm^{-2}, a slight effect of MO removal was observed. In consideration of electrolyte consumption and MO removal, the 20 mA cm^{-2} current density was chosen for the further studies.

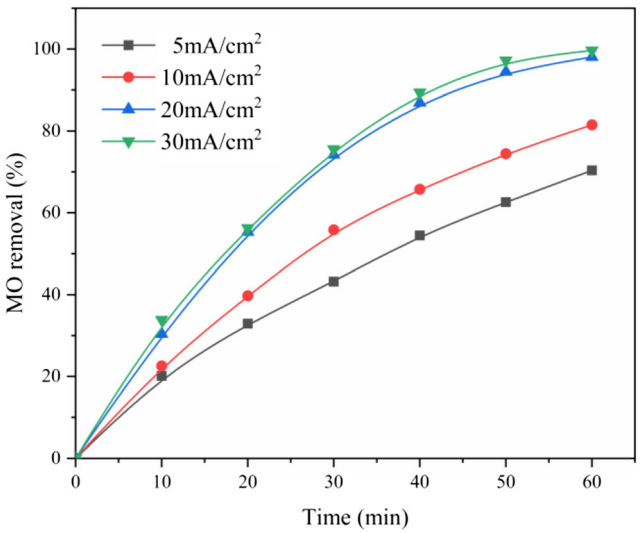

Fig. 12 Effect of initial current density on the MO degradation at initial pH = 5.0, 60 mg L^{-1} initial concentration, 0.15 mol L^{-1} Na_2SO_4 concentration, and 60 min of electrolysis time

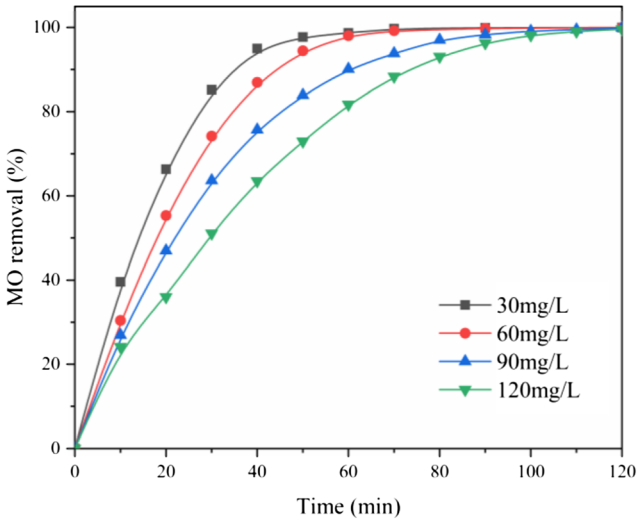

Fig. 13 Effect of initial concentration of MO on the degradation at initial pH = 5.0, 20 mA cm^{-2} current density, 0.15 mol L^{-1} Na_2SO_4 concentration, and 60 min of electrolysis time

Effect of initial dye concentration

The effect of initial MO concentration on the degradation is shown in Fig. 13. As can be seen from the figure, less time was spent to achieve a high removal as the initial MO concentration increases from 30 to 120 mg L^{-1}. The initial MO concentration of 60 mg L^{-1} was used in the studies.

Conclusions

In this paper, a Ti/SnO_2-Sb_2O_3/α-PbO_2/Ce-Nd-β-PbO_2 composite electrode was successfully prepared by the electrodeposition method. The proportion of Ce and Nd in the electrodeposition bath of Ce-Nd co-doped PbO_2 electrodes was optimized to 0.1 g L^{-1} $Ce(NO_3)_3$ and 0.2 g L^{-1} $Nd(NO_3)_3$ in terms of the MO and COD removals. The structure of Ce-Nd co-doped PbO_2 electrode was compared with those of the undoped and single-doped PbO_2 electrodes, and the crystal size of Ce-Nd-PbO_2 electrode was found to be smaller than the other PbO_2 electrodes from the results of SEM and XRD. The images of EDX and XPS have indicated that Ce and Nd were perfectly incorporated onto the surface of the PbO_2 electrode. The Ce-Nd-PbO_2 electrode showed the highest activity for the methyl orange by electrochemical oxidation. The MO and COD removals after 70 min of electrolysis were 99.8% and 100%, respectively. In addition, the Ce-Nd-PbO_2 electrode has the advantage of higher current efficiency and lower energy consumption.

Many studies have proven the doping of Ce or Nd in PbO_2 electrode can change the crystal structure and improve the electrochemical activity [4, 22, 33, 35, 36]. In this study, the Ce-Nd co-doped PbO_2 electrode has shown better catalytic

activity, and the improved performance of the modified electrode may be due to the dopants that changed the crystallite size and slowed down the deposition rate of PbO_2 crystal, but the specific mechanism needs further study. In conclusion, the Ce and Nd co-doped PbO_2 electrode can be considered a promising electrode for electrochemical oxidation of organic pollutants due to its high electrocatalytic activity and long service life.

Funding information This work was supported by the National High Technology Research and Development Program of China (863 Program) (no. 2012AA063504), the National Natural Science Foundation of China (nos. U1407116, 21511130020, and 21276193), and the Tianjin Municipal Natural Science Foundation (no. 13JCZDJC35600).

References

1. Salazar R, Brillas E, Sirés I (2012) Finding the best Fe^{2+}/Cu^{2+} combination for the solar photoelectro-Fenton treatment of simulated wastewater containing the industrial textile dye Disperse Blue 3. Appl Catal B Environ 115–116(none):107–116
2. Crini G (2006) Non-conventional low-cost adsorbents for dye removal: a review. Bioresour Technol 97(9):1061–1085
3. Brillas E, Martínez-Huitle CA (2015) Decontamination of wastewaters containing synthetic organic dyes by electrochemical methods. An updated review. Appl Catal B Environ 166-167: 603–643
4. Lyu J, Han H, Wu Q (2019) Enhancement of the electrocatalytic oxidation of dyeing wastewater (reactive brilliant blue KN-R) over the Ce-modified Ti-PbO_2 electrode with surface hydrophobicity. J Solid State Electrochem 23(3):847–859
5. Pan G, Jing X, Ding X (2019) Synergistic effects of photocatalytic and electrocatalytic oxidation based on a three-dimensional electrode reactor toward degradation of dyes in wastewater. J Alloys Compd:151749
6. Do JS, Chen ML (1994) Decolourization of dye-containing solutions by electrocoagulation. J Appl Electrochem 24(8):785–790
7. Yuan JG, Wang BR, Wang CD (2012) Study on treatment of dye wastewater by UASB-biological contact oxidation process. Adv Mater Res 627:390–393
8. Cotillas S, Llanos J, Cañizares P (2018) Removal of Procion Red MX-5B dye from wastewater by conductive-diamond electrochemical oxidation. Electrochim Acta 263:1–7
9. Sirés I, Brillas E, Oturan M (2014) Electrochemical advanced oxidation processes: today and tomorrow. A review. Environ Sci Pollut Res 21(14):8336–8367
10. Ferreira MB, Rocha JHB, Da Silva DR (2016) Application of electrochemical oxidation process to the degradation of the Novacron Blue dye using single and dual flow cells. J Solid State Electrochem 20(9):2589–2597
11. Labiadh L, Barbucci A, Cerisola G (2015) Role of anode material on the electrochemical oxidation of methyl orange. J Solid State Electrochem 19(10):3177–3183
12. Labiadh L, Barbucci A, Carpanese MP (2017) Direct and indirect electrochemical oxidation of indigo carmine using PbO_2 and $TiRuSnO_2$. J Solid State Electrochem 21(8):2167–2175
13. Zhu S, Dong B, Zhou S (2018) Degradation of atenolol with electrochemical oxidation at mixed metal oxide electrodes assisted by UV photolysis. Clean-Soil Air Water 46(4):1700077
14. Qiao MX, Zhang Y, Zhai LF (2018) Corrosion of graphite electrode in electrochemical advanced oxidation processes: degradation protocol and environmental implication. Chem Eng J 344:410–418
15. Borras N, Oliver R, Arias C (2010) Degradation of atrazine by electrochemical advanced oxidation processes using a boron-doped diamond anode. J Phys Chem A 114(24):6613–6621
16. Chaplin BP (2014) Critical review of electrochemical advanced oxidation processes for water treatment applications. Environmental Science Processes & Impacts 16(6):1182–1203
17. Vilar V, Brillas E, Boaventura R (2017) Electrochemical advanced oxidation processes: a review on their application to synthetic and real wastewaters. Appl Catal B Environ 202:217–261
18. Panizza M, Cerisola G (2009) Direct and mediated anodic oxidation of organic pollutants. Chem Rev 109(12):6541–6569
19. Jum'h I, Abdelhay A, Telfah A (2018) Veratric acid removal from water by electrochemical oxidation on BDD anode. IOP Conference Series: Materials Science and Engineering 305:012021
20. Candia-Onfray C, Espinoza N, Silva EBSD (2018) Treatment of winery wastewater by anodic oxidation using BDD electrode. Chemosphere 206:709–717
21. Zahorulko S, Shmychkova O, Luk'Yanenko T (2019) The comparative study of electrocatalytic activity of various anode materials in respect to the oxidation of nitroanilines. Materials Today-Proceedings 6(2):242–249
22. Hu X, Yu Y, Yang L (2015) Electrocatalytic activity of Ce-PbO_2/C anode for acid red B reduction in aqueous solution. J Solid State Electrochem 19(6):1599–1609
23. Pereira JF, Figueiredo RS, Ponce-de-León C (2016) Platinum-free lead dioxide electrode for electrooxidation of organic compounds. J Solid State Electrochem 20(4):1167–1173
24. Zaidi SZJ, Harito C, Walsh FC (2018) Decolourisation of reactive black-5 at an RVC substrate decorated with PbO_2/TiO_2 nanosheets prepared by anodic electrodeposition. J Solid State Electrochem 22(9):2889–2900
25. Santos JEL, de Moura DC, Da Silva DR (2019) Application of TiO_2-nanotubes/PbO_2 as an anode for the electrochemical elimination of Acid Red 1 dye. J Solid State Electrochem 23(2):351–360
26. Shmychkova O, Luk'Yanenko T, Yakubenko A (2015) Electrooxidation of some phenolic compounds at Bi-doped PbO_2. Appl Catal B Environ 162:346–351
27. Wang C, Niu J, Yin L (2018) Electrochemical degradation of fluoxetine on nanotube array intercalated anode with enhanced electronic transport and hydroxyl radical production. Chem Eng J 346: 662–671
28. Zheng Y, Su W, Chen S (2011) Ti/SnO_2-Sb_2O_5-RuO_2/α-PbO_2/β-PbO_2 electrodes for pollutants degradation. Chem Eng J 174(1): 304–309
29. Duan X, Xu F, Wang Y (2018) Fabrication of a hydrophobic SDBS-PbO_2 anode for electrochemical degradation of nitrobenzene in aqueous solution. Electrochim Acta 282:662–671
30. Zhang W, Kong H, Lin H (2015) Fabrication, characterization and electrocatalytic application of a lead dioxide electrode with porous titanium substrate. J Alloys Compd 650:705–711
31. Zhou K, Tian Y, Ma H (2018) Photoelectrocatalytic performance of conductive carbon black-modified Ti/F-PbO_2 anode for degradation of dye wastewater (reactive brilliant blue KN-R). J Solid State Electrochem 22(4):1131–1141
32. Li H, Chen Y, Zhang Y (2013) Preparation of Ti/PbO_2-Sn anodes for electrochemical degradation of phenol. J Electroanal Chem 689: 193–200
33. Zhang C, Liu J, Chen B (2019) Effect of Ce(NO3)(4) on the electrochemical properties of Ti/PbO_2-TiO_2-Ce(NO3)(4) electrode for zinc electrowinning. Applied Physics A-Materials Science & Processing 125:150

34. Liu H, Yu S, Shen T (2014) Preparation of a high-performance composite PbO_2 electrode from a new bath for p-chlorophenol oxidation. Sep Purif Technol 132:27–32
35. Chen Z, Yu Q, Liao D (2013) Influence of nano-CeO_2 on coating structure and properties of electrodeposited Al/α-PbO_2/β-PbO_2. Trans Nonferrous Metals Soc China 23(5):1382–1389
36. Yao Y, Huang C, Yang Y (2018) Electrochemical removal of thiamethoxam using three-dimensional porous PbO_2-CeO_2 composite electrode: electrode characterization, operational parameters optimization and degradation pathways. Chem Eng J 350:960–970
37. Yu H, Song Y, Zhao B (2018) Efficient electrocatalytic degradation of 4-chlorophenol using a Ti/RuO_2-SnO_2-TiO_2/PbO_2-CeO_2 composite electrode. Electrocatalysis 9(6):725–734
38. Xu M, Mao Y, Song W (2018) Preparation and characterization of Fe-Ce co-doped Ti/TiO_2 NTs/PbO_2 nanocomposite electrodes for efficient electrocatalytic degradation of organic pollutants. J Electroanal Chem 823:193–202
39. Zhang Y, He P, Jia L (2019) Ti/PbO_2-Sm_2O_3 composite based electrode for highly efficient electrocatalytic degradation of alizarin yellow R. J Colloid Interface Sci 533:750–761
40. Yao Y, Teng G, Yang Y (2019) Electrochemical oxidation of acetamiprid using Yb-doped PbO_2 electrodes: electrode characterization, influencing factors and degradation pathways. Sep Purif Technol 211:456–466
41. Yao Y, Li M, Yang Y (2019) Electrochemical degradation of insecticide hexazinone with Bi-doped PbO_2 electrode: influencing factors, intermediates and degradation mechanism. Chemosphere 216: 812–822
42. Wang X, Wu Q, Ma H (2019) Fabrication of PbO_2 tipped Co_3O_4 nanowires for efficient photoelectrochemical decolorization of dye (reactive brilliant blue KN-R) wastewater. Sol Energy Mater Sol Cells 191:381–388
43. Yao Y, Ren B, Yang Y (2019) Preparation and electrochemical treatment application of Ce-PbO_2/ZrO_2 composite electrode in the degradation of acridine orange by electrochemical advanced oxidation process. J Hazard Mater 361:141–151
44. Chen B, Yan W, He Y (2019) Influence of F-doped beta-PbO_2 conductive ceramic layer on the anodic behavior of 3D Al/Sn rod Pb-0.75% Ag for zinc electrowinning. J Electrochem Soc 166(4): E119–E128
45. Xia Y, Dai Q (2018) Electrochemical degradation of antibiotic levofloxacin by PbO_2 electrode: kinetics, energy demands and reaction pathways. Chemosphere 205:215–222
46. Weng M (2018) Electrochemical oxidation of tetracaine hydrochloride using a transition metal doped PbO_2 electrode. Int J Electrochem Sci 13(12):11720–11729
47. Du H, Duan G, Wang N (2018) Fabrication of Ga_2O_3-PbO_2 electrode and its performance in electrochemical advanced oxidation processes. J Solid State Electrochem 22(12):3799–3806
48. Gurung K, Ncibi MC, Shestakova M (2018) Removal of carbamazepine from MBR effluent by electrochemical oxidation (EO) using a Ti/Ta_2O_5-SnO_2 electrode. Appl Catal B Environ 221:329–338
49. Jin Y, Wang F, Xu M (2015) Preparation and characterization of Ce and PVP co-doped PbO_2 electrode for waste water treatment. J Taiwan Inst Chem Eng 51:135–142
50. Ansari A, Nematollahi D (2018) A comprehensive study on the electrocatalytic degradation, electrochemical behavior and degradation mechanism of malachite green using electrodeposited nanostructured beta-PbO_2 electrodes. Water Res 144:462–473
51. Qiao Q, Singh S, Lo S (2018) Electrochemical oxidation of acid orange 7 dye with Ce, Nd, and Co-modified PbO_2 electrodes: preparation, characterization, optimization, and mineralization. J Taiwan Inst Chem Eng 84:110–122
52. Shmychkova O, Luk Yanenko T, Amadelli R (2016) Electrodeposition of Ni^{2+}-doped PbO_2 and physicochemical properties of the coating. J Electroanal Chem 774:88–94
53. Chang L, Zhou Y, Duan X (2014) Preparation and characterization of carbon nanotube and Bi co-doped PbO_2 electrode. J Taiwan Inst Chem Eng 45(4):1338–1346
54. Duan X, Zhao Y, Liu W (2014) Electrochemical degradation of p-nitrophenol on carbon nanotube and Ce-modified-PbO_2 electrode. J Taiwan Inst Chem Eng 45(6):2975–2985
55. Shmychkova O, Luk Yanenko T, Piletska A (2015) Electrocrystallization of lead dioxide: influence of early stages of nucleation on phase composition. J Electroanal Chem 746:57–61
56. Shmychkova O, Luk Yanenko T, Amadelli R (2014) Physicochemical properties of PbO_2-anodes doped with $Sn^{4+}$and complex ions. J Electroanal Chem 717-718:196–201
57. Shmychkova O, Luk Yanenko T, Amadelli R (2013) Electrodeposition of Ce-doped PbO_2. J Electroanal Chem 706: 86–92